Chapter 5

Effects of Joints in Reaction Rail on the Thrust of LIM

5.1 Introduction

In this chapter, effects of Joints in reaction rail and back-iron and proximity of ferromagnetic material on the thrust of Linear Induction Motor have been investigated. In Linear Induction Motor (LIM) thrust production is affected due to local conditions of reaction rail. Any break in the path of eddy currents affects the performance of LIM. Furthermore, the presence of ferromagnetic material in the air-gap changes the eddy current pattern in conducting sheet and thereby affects the force production. This chapter investigates the effect of a single joint in conducting sheet and back iron on the generated thrust and normal force under standstill and dynamic conditions by analyzing the secondary eddy current density and the air-gap flux density distributions along the x-direction with the 2D-FEM simulation carried out on Ansys Maxwell software. The results can be further used for finding a better alternative of reaction rail.

A hybrid reaction rail having the convenience of a sheet secondary and advantages of squirrel cage must be sought. In an elementary form such a secondary will have

jutted ferromagnetic and conducting material both present in the air gap. The presence of ferromagnetic material in the clearance changes the eddy current pattern in conducting sheet and thereby affects the force production. This chapter further analyzes the effect of presence of a thin ferromagnetic strip in the clearance of SLIM on its thrust production. The results can be further used for finding a better alternative of LIM secondary.

5.2 The 2-D FEM model of LIM

Variable frequency harmonic analysis has been carried out as reported in [59] for validating the 2D-FEM model created with the same parametric dimensions as in [59] and depicted in Fig. 5.1. The design parameter details are given in Table 5.1 . The 5 pole, half-filled end slots stator houses coils with 70 turns each and the instantaneous positive polarity of current excitation is indicated by the dots. The subsequent pole pitches $(\tau - 5\tau)$ are also marked against their lengths from the entry side edge towards the exit side edge of the primary as seen by the travelling magnetic field. The secondary sheet is taken to be touching and below the x - z plane, above which are airgap and the stator. The variable frequency standstill simulation results bearing striking resemblance with those of [59], pave the way for corroboration.

Fig. 5.1 also displays the flux density (absolute magnitudes) distribution along the teeth and slots of the whole length of the stator surface at the instant of 2 ms after the commencement of excitation of a constant current of 3 A (rms). In contrast to the expected general trend of the flux density to be a minimum at the slot openings and peaking at the tooth tips with the average value being at the tooth centers, there is some degree of distortion because of the cross magnetization of the flux due to the interaction of the mmfs of the primary and the secondary currents.

Fig. 5.2 illustrates the standstill thrust on the secondary at different frequencies which corresponds to the result obtained in [59] for the slotted model with the Russel and

Table 5.1 2D LIM Design parameter details

Parameter	Value
Length of LIM (x-direction)	312 mm
Stator thickness (y-direction)	50 mm
Depth of the 2D model (z-direction)	60 mm
Number of poles	5
Pole Pitch	62.4 mm
Number of slots	15
Number of turns per coil	70
Slot width	15.8 mm
Slot depth	31.2 mm
Clearance	3.66 mm
Thickness of conducting sheet	1.94 mm
Primary current (rms)	3 A
Conductivity of the secondary sheet	3.59×10^7 S/m

Norsworthy correction [60] for the plate resistivity. The result obtained in [59] for the current sheet model can be calculated analytically by Parseval's method of 3D Fourier Transform applicable for LIM [45] with no back-iron and briefed in [61], [62] for the method of numero-analytical integration.

Fig. 5.3 projects the secondary conductive sheet instantaneous z-directed eddy current densities against the stator length during a half Time Period. The subsequent current distributions corresponding to the indicated time instances illustrate the direction of progress of the travelling magnetic field wave.

5.3 Effect of joint in secondary conducting sheet and back iron

In this section, the effect of a single joint in conducting sheet and back iron on the generated thrust and normal force under standstill and dynamic conditions has been investigated. A 2D FEM model of LIM having a joint in conducting sheet and back iron taking slots into account has been developed. This has been shown in Fig 5.4. The details of the analyzed

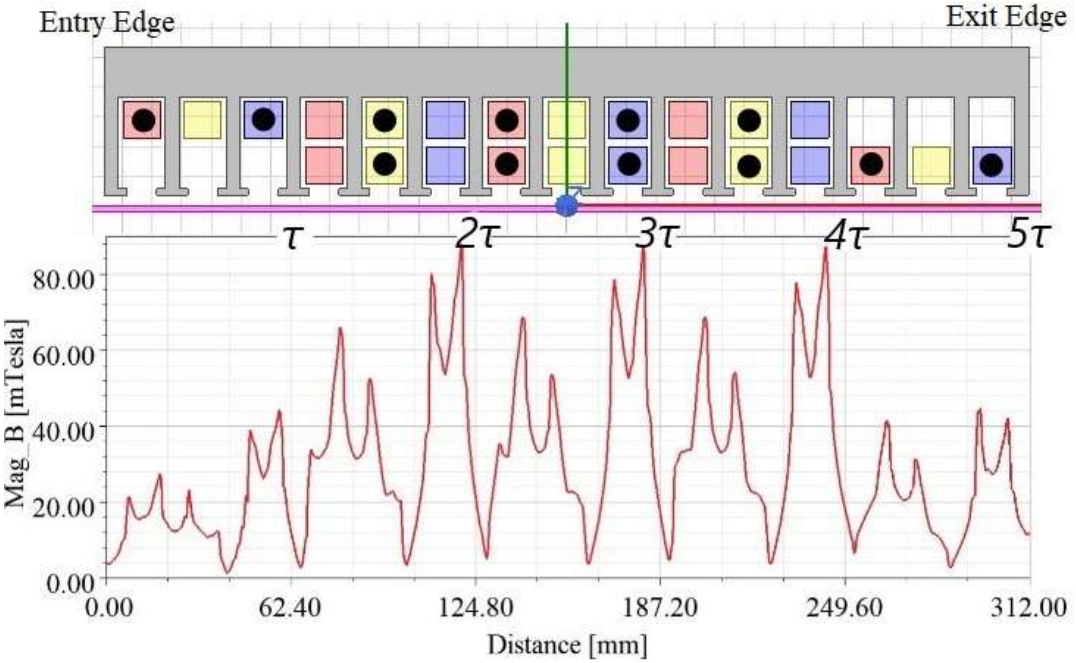

Fig. 5.1 Flux density distribution at the stator surface, at 50 Hz

LIM are the same as given in Table 5.1. The Conductivity of the un-laminated back-iron was chosen to be 1.05×10^6 S/m [48]. The thickness of the backiron is 8 mm. The steady state analysis has been done for a constant current of 3 Ampere and a supply frequency of 60 Hz. Two cases have been investigated: (1) composite reaction rail with a joint in (a) conducting sheet and (b) back iron; (2) reaction rail having plain conducting sheet with a joint. In all these cases the joint is of 3.0 mm size in longitudinal direction.

5.3.1 Effect of joint under Dynamic condition

Fig. 5.4 is schematic in nature, while the Simulation Model setup is detailed in Table 5.2. The positions of the joints in the secondary conductive sheet and back-iron are also tabulated in it.

Fig. 5.5 lays out the magnitudes of flux density distribution along the teeth and slots of the whole length of the stator surface at the instant of 2 ms as obtained in the 3D

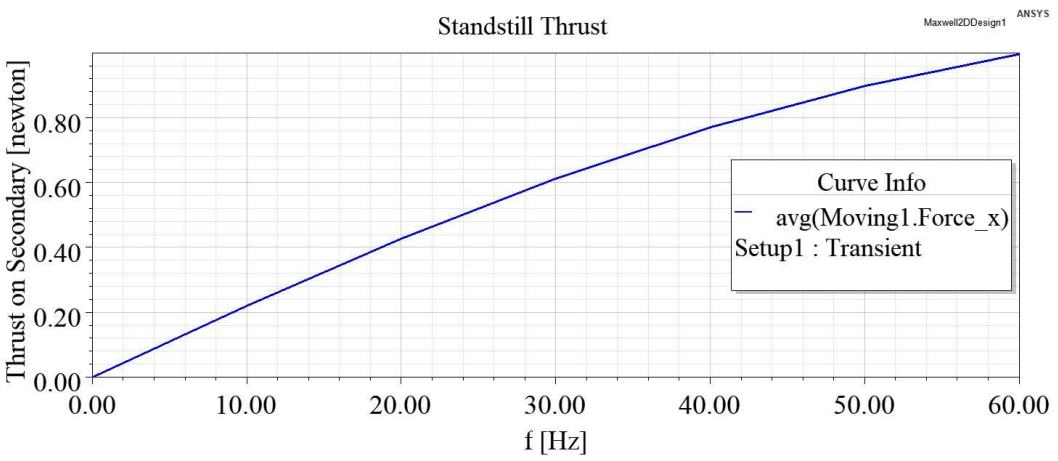

Fig. 5.2 Standstill Thrust at different frequencies, at 50 Hz

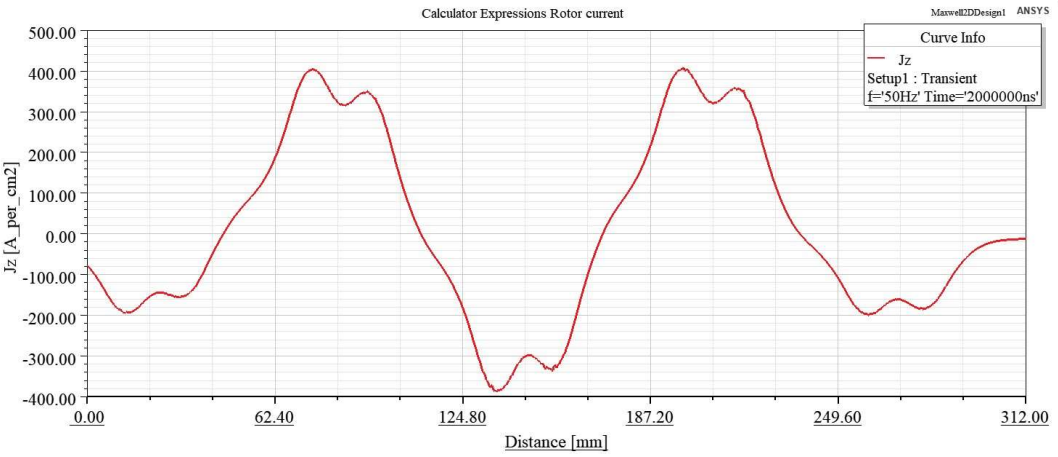

Fig. 5.3 Rotor current density distributions during one half Time Period at 50 Hz

FEM simulation model. The width of the secondary is 130 mm [59]. The 3-dimensional simulation couldn't be performed for an Analysis run time of more than 6 ms as it took exorbitant storage space and time and got aborted. Hence, the analysis has been carried out on 2D FEM model. Fig. 5.6 is the 2D counterpart of Fig. 5.5 and is in fairly good agreement.

Fig. 5.7 shows the eddy current (absolute values) distribution at the sheet surface of the air-gap-secondary interface, while Fig. 5.8 is the 2D counterpart. It may be noted here that the magnitudes depicted in the 3D plot is the vector sum of both the x and z-components,

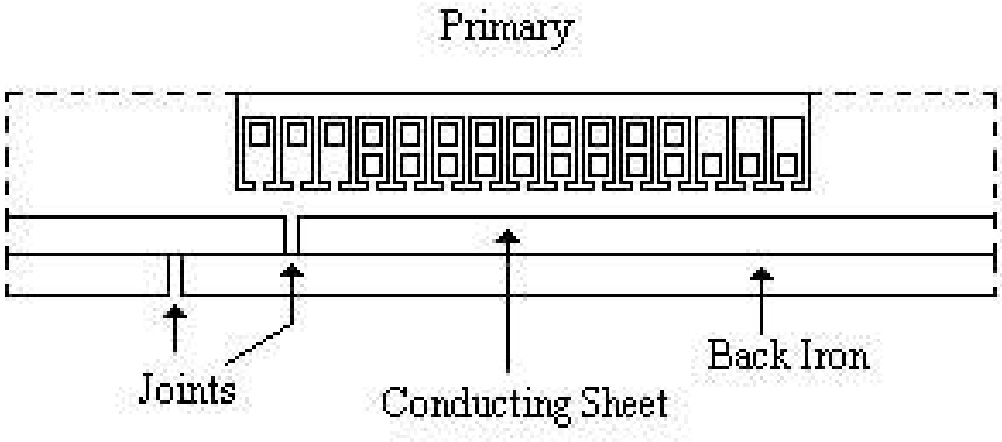

Fig. 5.4 A schematic 2D model of SLIM with joints in Reaction Rail

Table 5.2 Simulation Setup details

Parameter	**Value**
Analysis Run time	1750 ms
Evaluation Time step	1 ms
Translation limit	1700 mm
Velocity of translation of the secondary member of LIM)	1 m/s
X-coordinates of the ends of stator of LIM	0 mm & 312 mm
X-coordinates of the ends of secondary of LIM	−1447 mm & 316 mm
X-coordinates of the ends of joint in the secondary sheet	−544 mm & −541 mm
X-coordinates of the ends of joint in the secondary back-iron	−944 mm & −941 mm

while the 2D plot takes into account only the z-component of eddy current. The red curve in Fig. 5.8 represents the absolute value of the eddy current magnitude.

A pictorial view of the eddy current paths in the secondary sheet parallel to the *x*-z plane is laid out in Fig. 5.9 indicated by the current density vectors. The density of eddy currents is of the order of 10^6 A/m^2. The map of the eddy current paths in the un-laminated secondary back-iron is shown in Fig. 5.10. The density of the eddy currents is of the order of $10^{-7} - 10^{-8}$ A/m^2.

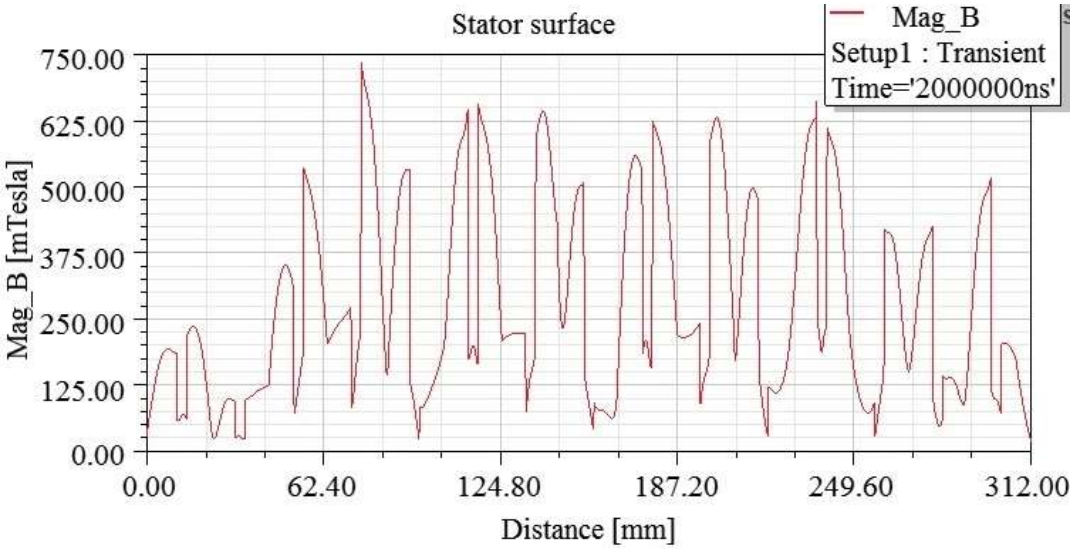

Fig. 5.5 3-D Flux density distribution at the Stator surface

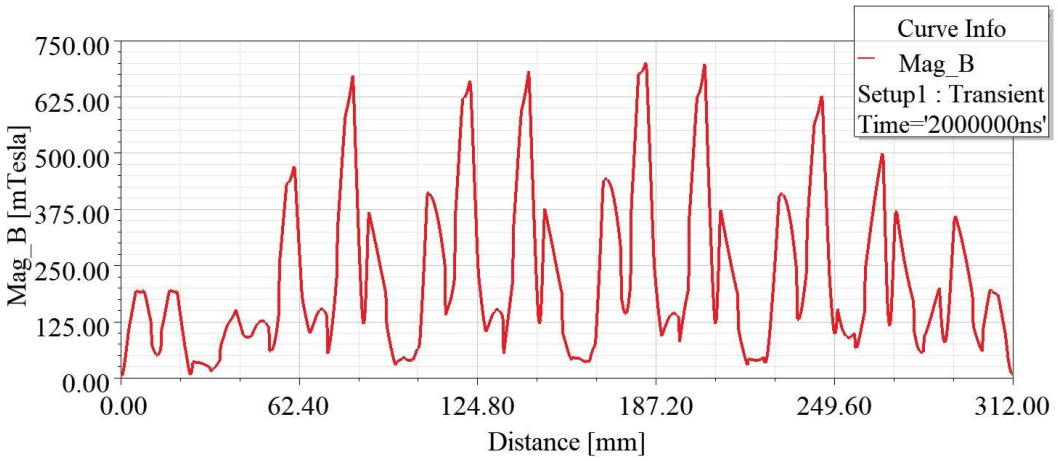

Fig. 5.6 2-D Flux density distribution at the Stator surface

Fig. 5.11 portrays the effect on thrust due to joints in the conductive sheet and back-iron, when the secondary is moving from left to right (direction of the travelling magnetic field) at a constant speed of 1 m/s. The red curve represents the thrust experienced by the primary stator which would translate to perturbance (vibration), while the green curve is the reaction observed by the secondary member. The solid straight blue line represents the distance moved by the secondary, the markers on which are elaborated in Table 5.3.

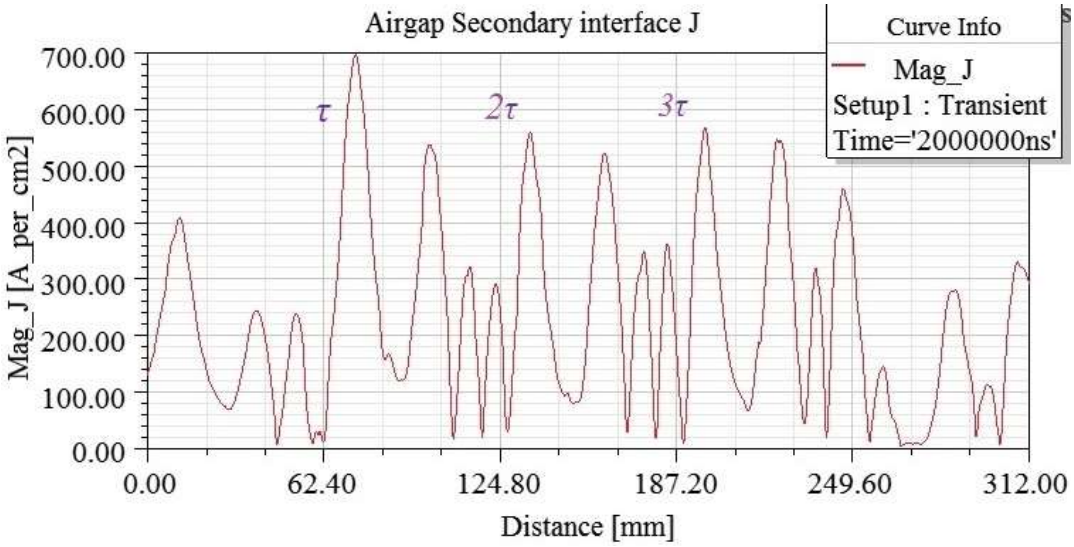

Fig. 5.7 3D surface current density distribution at Air-gap and Secondary interface

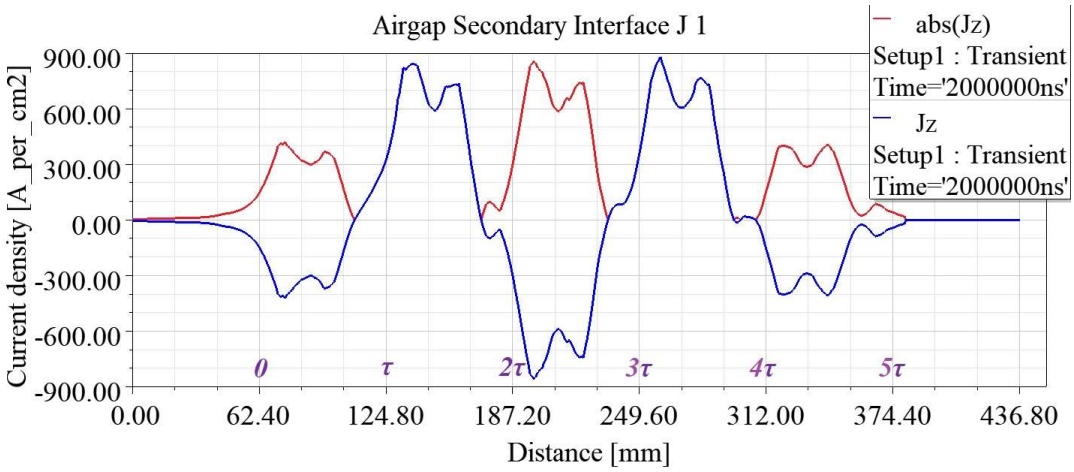

Fig. 5.8 2D surface current density distribution at Air-gap and Secondary interface

At rest the secondary member is just edging past the primary in the positive x-direction by a mere 4 mm as indicated by Table 5.2 . The eddy currents produced in the secondary conductive sheet under the active width (w) of the stator is z-directed in ideal case and the return paths are x-directed in the secondary overhangs [6]. Moreover, in 2D analysis, the z-directed currents are only taken into account. Hereafter, the eddy currents within the width w along the entire length of the secondary will only be considered. When the

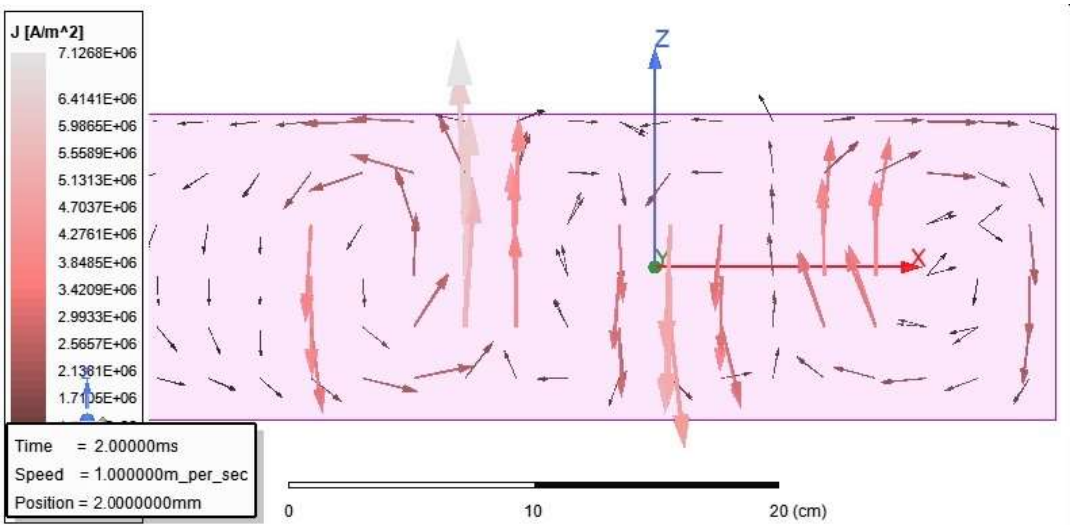

Fig. 5.9 3D pictorial map of eddy current density in the Secondary sheet

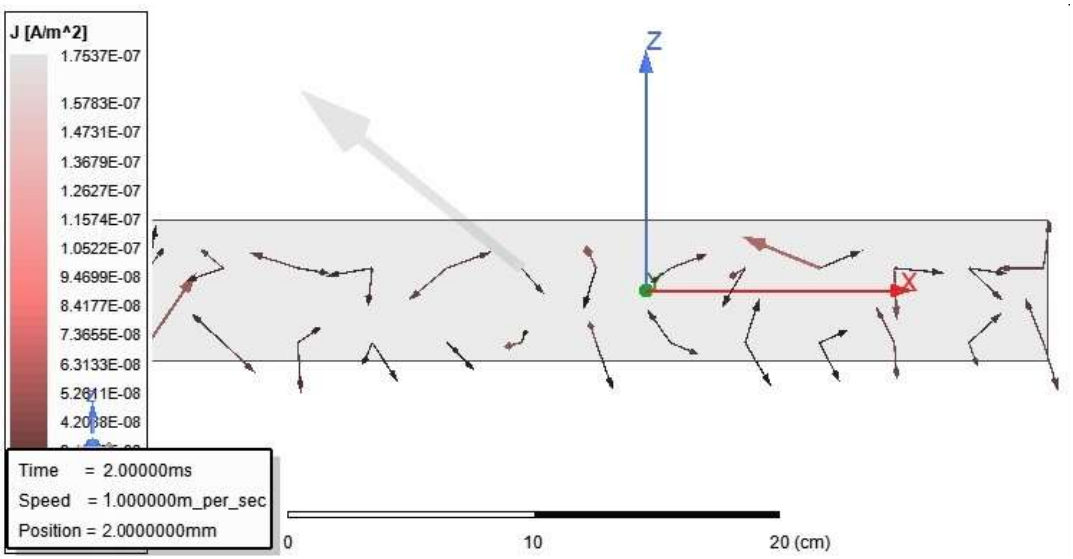

Fig. 5.10 3D pictorial map of eddy current density in the Secondary back-iron

secondary sets into motion with a constant velocity of 1 m/s in the positive x-direction (towards right), the density of eddy currents generated near the rightmost (exit) edge of the secondary sheet still has a dominant z-component (x-component being restricted by the end of the sheet). On further movement, the eddy currents fringe out progressively in the x-direction (now no more restricted) beyond the active zone of the secondary under the

Table 5.3 Coordinates of the markers in Fig. 5.11

Marker Number	X (s)	Y (mm)
M1	0.312	312
M2	0.541	541
M3	0.853	853
M4	0.941	941
M5	1.253	1253
M6	1.447	1447

primary stator, typically like that at the entry edge as depicted in Fig. 5.9. This weakens the z-component of the eddy currents density as depicted in Fig. 5.12.

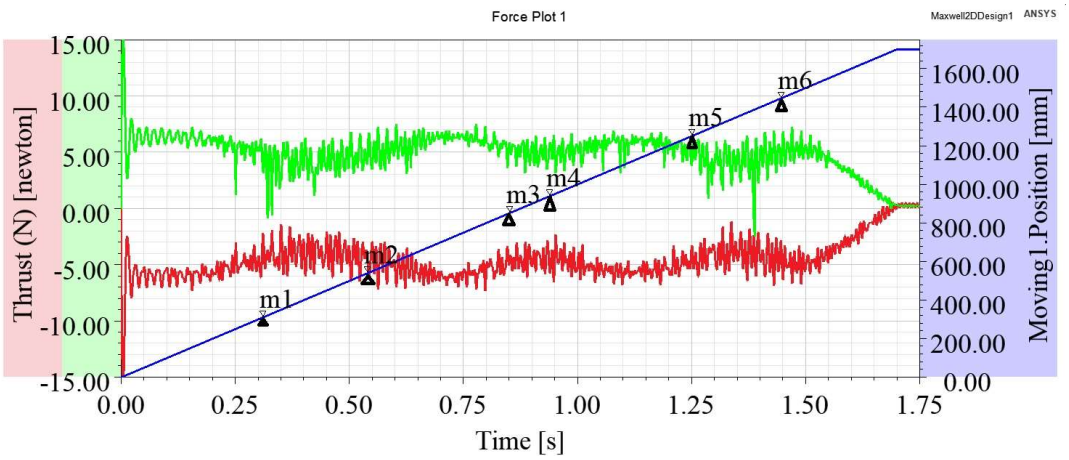

Fig. 5.11 Thrust for joints in Reaction Rail under Dynamic condition

In Fig. 5.11, the magnitude of thrust begins to droop until the marker M1 (Table 5.3), at which point, the secondary has moved by a distance equal to the exact length of the stator. After M1 the thrust is constant up to M2 whereon the joint in the secondary sheet reaches the entry edge as indicated in Table 5.2. The magnitude of the thrust swells as the joint moves under the entire length of the stator in the zone between M2 and M3, whereupon the joint in the sheet gets past the exit end of the stator and the thrust has subsided. Between M3 and M4, thrust remains constant until the joint in the back-iron appears at the entry edge. The magnitude of the thrust again swells (though to a lesser degree) as the joint in the back-iron moves under the entire length of the stator between M4 and M5, at which

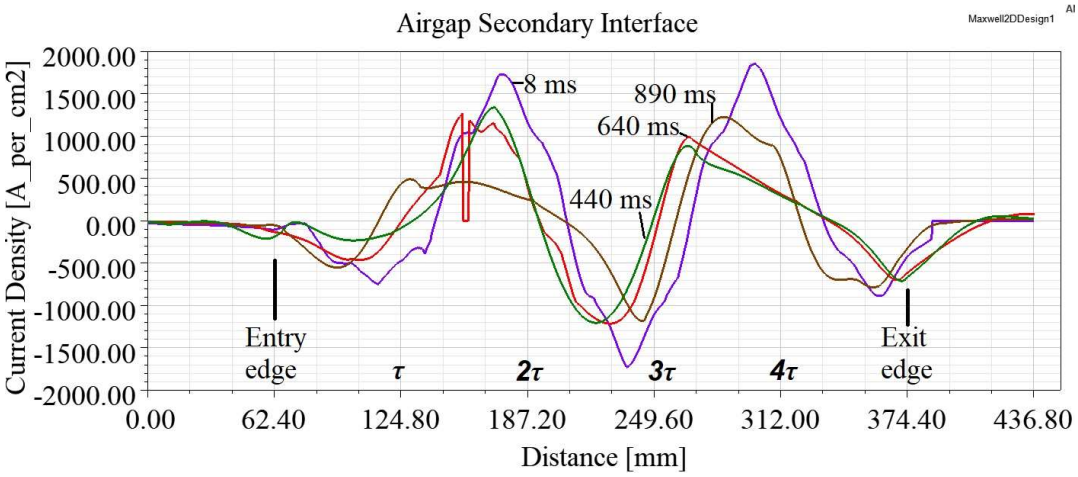

Fig. 5.12 Eddy current densities at the Air-gap and secondary sheet interface at different instances of translation of the secondary

point the joint in the sheet gets past the exit end of the stator and the thrust subsides. In the zone between M5 and M6, the length of the secondary left beyond the entry edge is (1447 - (1253+ 3) = 191 mm), which is less than the stator length. Hence, the thrust again begins to swell beyond M5 in a reverse manner corresponding to M1 0 . At M6, the end of the secondary has reached the entry edge, whereupon the active length of the secondary under the primary progressively decreases, thereby diminishing the thrust linearly and becomes zero just before the translation limit of 1.7 m is achieved making the standstill thrust also zero for another 5 ms of the remaining analysis run time with about a length of the secondary equivalent to one pole pitch still remaining inside the exit end.

Barring the purple curve (8 ms) in Fig. 5.12, all the other curves are displaced from each other by multiples of the Time Period (16.67 ms) and hence are in the same phase for the sake of comparison.

Fig.5.12 exhibits the eddy current densities on the surface of the sheet secondary at the air-gap and secondary interface for four instances corresponding to the four zones described in Table 5.4 and the remaining two instances are pictured in Fig. 5.13 separately for the sake of clarity.

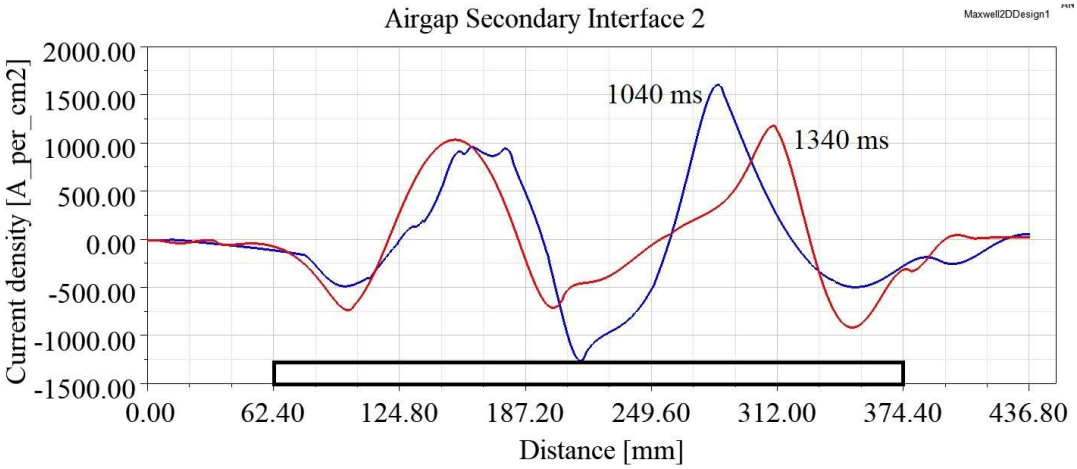

Fig. 5.13 Eddy current densities at the Air-gap and secondary sheet interface at different instances (contd.)

Table 5.4 Eddy current densities at the Air-gap and secondary sheet interface at different instances

Curve color	Zone	Time (s)	$J_Z\,(\mathbf{A/cm^2})$ **rms**
Fig. 5.12			
	0– M1	0.008	795
	M1 - M2	0.440	519
	M2 - M3	0.640	551
	M3 - M4	0.890	515
Fig. 5.13			
	M4 - M5	1.040	581
	M5 - M6	1.340	501

From Table 5.4, it can be inferred that the z- component of the eddy current density J_Z gets increased due to constriction of J_Z and restriction of J_X at the exit edge like in the starting (0.008 ms) and adjacent to joints when there is one in sheet (640 ms) or back-iron (1040 ms) of the secondary under active zone of the primary. This surge in J_z is responsible for the swelling of thrust for only the z component of eddy current interacting with the y component of flux density is responsible for thrust production [63].

Fig. 5.14 depicts the eddy current densities on the surface of the sheet secondary at the air-gap and secondary interface for four instances belonging to zone M2-M3, when the joint in the sheet secondary moves under the active zone of the stator. The eddy current

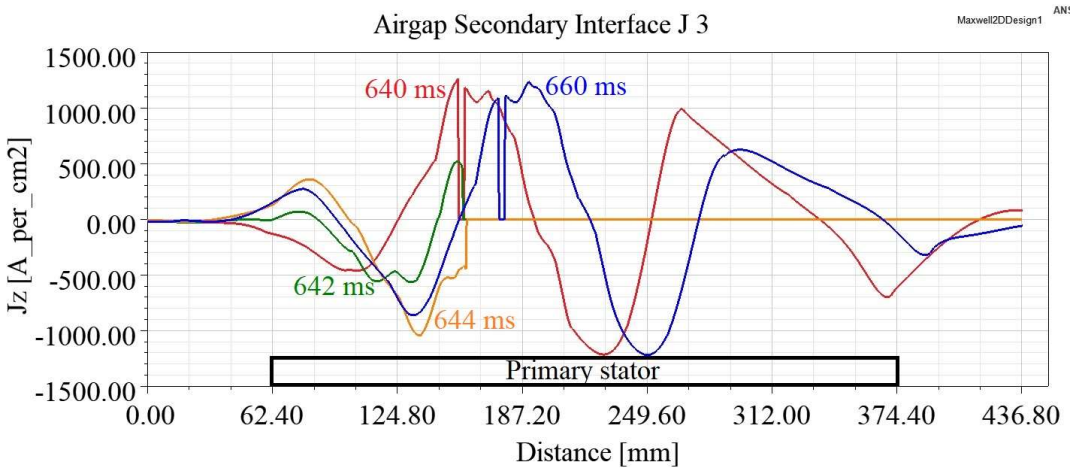

Fig. 5.14 Eddy current densities at the Air-gap and secondary sheet interface at different instances when the stator moves over the joint in the secondary sheet

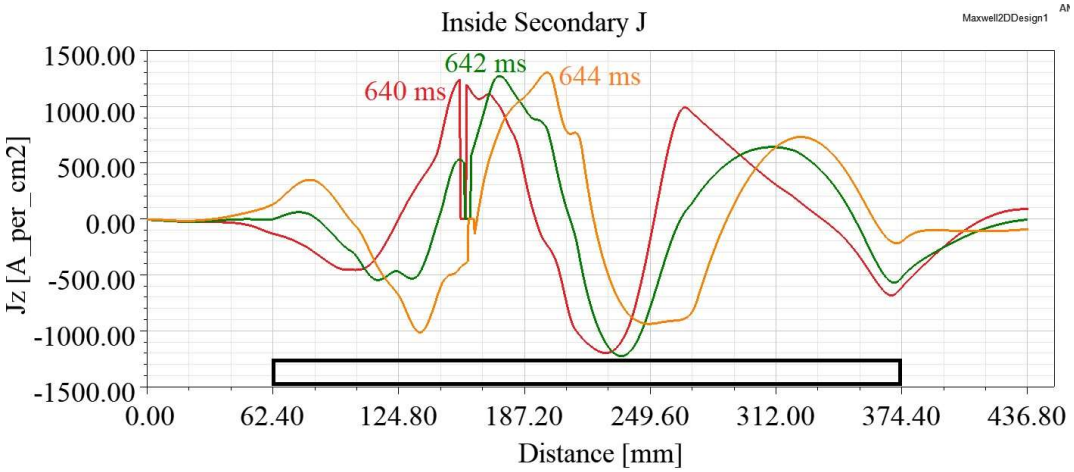

Fig. 5.15 Eddy current densities inside secondary sheet (half depth) at different instances when the stator moves over the joint in the secondary sheet

density J_Z curves pertaining to instances 640 ms and 660 ms exhibit a break of 3 mm, while at intermediate instances 642 ms and 644 ms, there is a complete break of flow of eddy current at the sheet surface forcing the currents to bulge inside the secondary sheet as is indicated by the squarish shape of the distribution in Fig. 5.15.

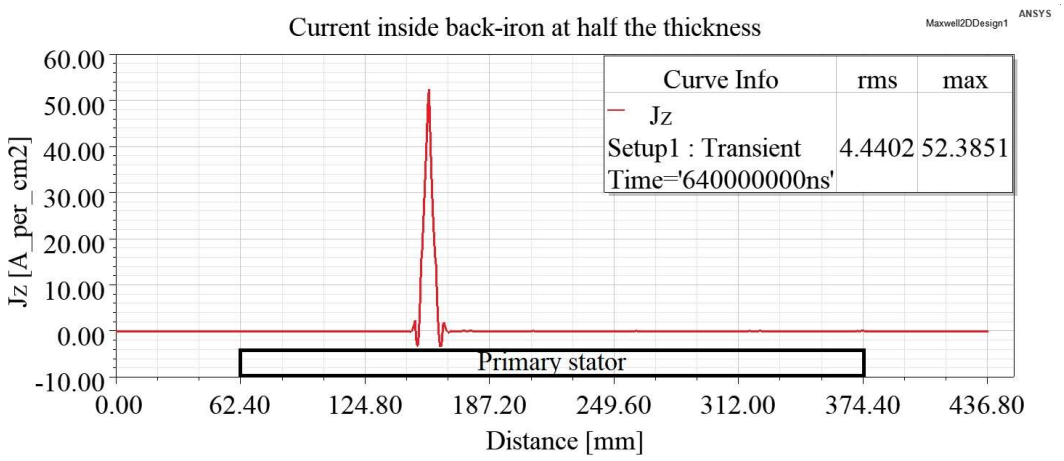

Fig. 5.16 Eddy current density inside secondary back-iron (half depth) at one instance (640 ms) when the joint in the secondary sheet is under the stator

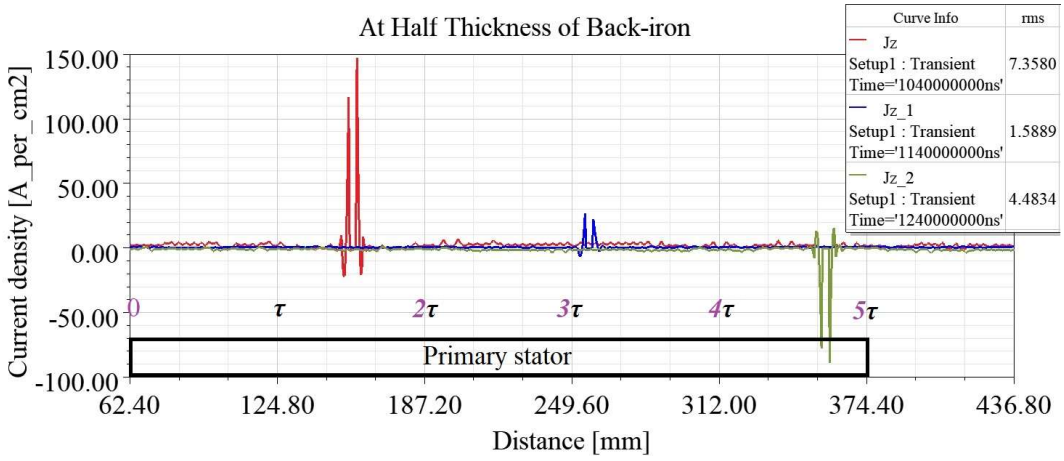

Fig. 5.17 Eddy current densities inside secondary back-iron (half depth) at different instances when the stator moves over the joint in the secondary back-iron

There also happens to be spikes in the eddy current density inside the back-iron as a reaction to a break in eddy current in the sheet secondary as at the instance 640 ms as shown in Fig. 5.16.

Fig. 5.17 exhibits the break in eddy current density along with the spikes adjacent to it when joint in the back-iron of the secondary comes under the active zone. This leads to the crowding (constriction) of flux adjacent to the joint as depicted in Fig. 5.18.

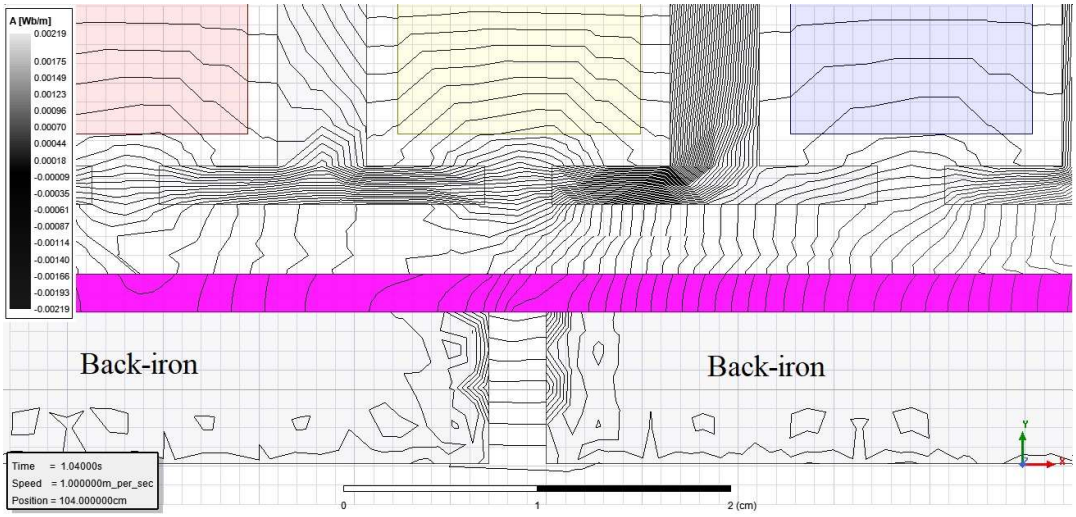

Fig. 5.18 Crowding of the flux near joint in the back-iron

Like Fig. 5.11 pertaining to thrust, Fig. 5.19 displays the normal direction force on the secondary (green curve) and primary (red curve), whose directions (+/-) indicate that they are attractive in nature. The normal force also goes through similar variations like those of the thrust. The z and x-component of eddy current interacting respectively with the x and z-component of flux density is responsible for the generation of normal direction force. But in 2D analysis, the x-component of eddy current and moreover, z-component of flux density aren't taken into account. This explains the exponential fall of the normal force in the initial period in contrast to the drooping thrust in the same period.

5.3.2 Effect of joint under Standstill condition

Three separate cases have been investigated for standstill conditions: (1) composite reaction rail with a joint in conducting sheet only and separately in (2) back iron only; (3) reaction rail having plain conducting sheet with a joint. In all these cases the joint is of 3.0 mm size in longitudinal direction like in the dynamic analysis and their thrust versus position characteristics are illustrated in Fig. 5.20, Fig. 5.21 and Fig. 5.22 respectively.

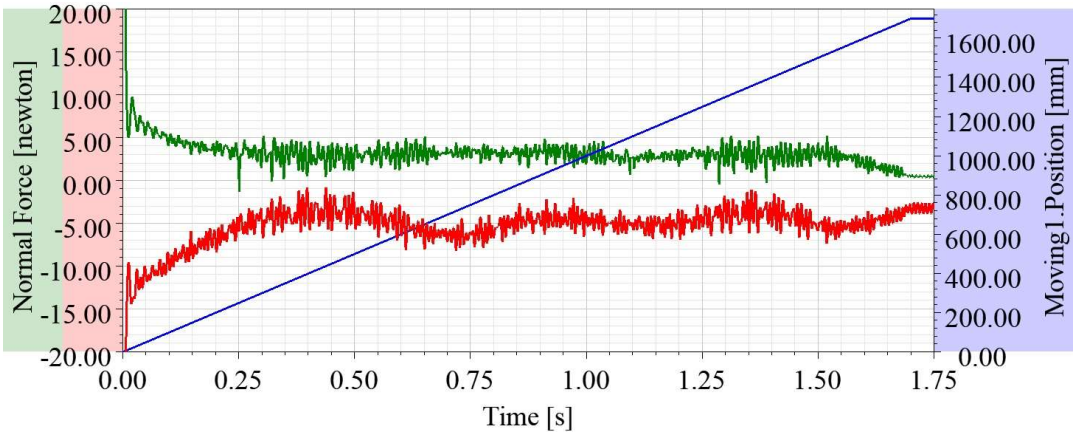

Fig. 5.19 Normal force for joints in Reaction Rail under Dynamic condition

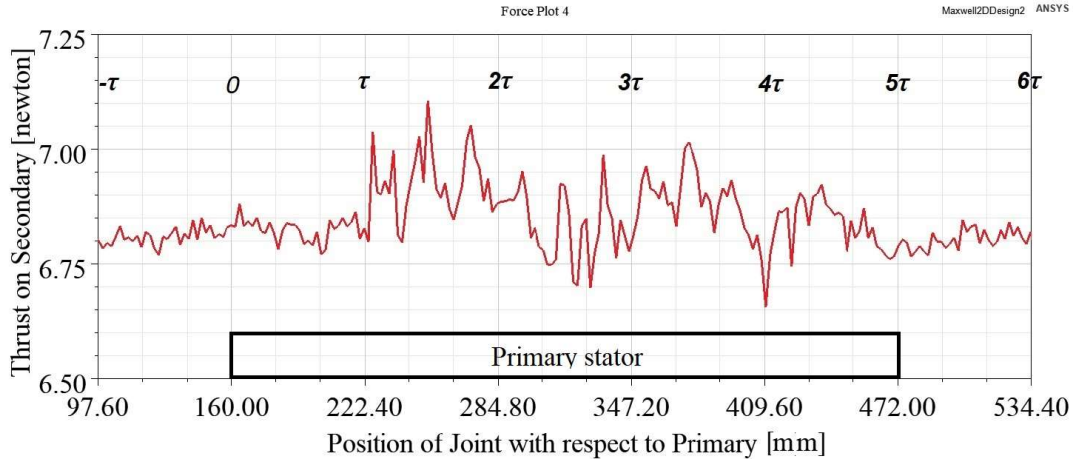

Fig. 5.20 Thrust on the composite secondary versus position of a single joint in the sheet with respect to LIM Primary

The magnitude of the standstill thrust is more than that of the average dynamic thrust. The standstill thrust ripples are also more pronounced when the joints come under active zone. In contrast, the dynamic thrust contains huge thrust ripples when the healthy portion of secondary is under the active zone of the primary (Fig. 5.19) and swells smoothly to

Another glaring observation is that, the perturbance and swell in the thrust isn't significant until the joint is within a distance of one pole pitch (τ) into the active zone from the entry edge. Beyond this and up to a distance of one pole pitch from the exit end, there is a marked rise in the magnitudes of ripples and average thrust owing to heavy restriction

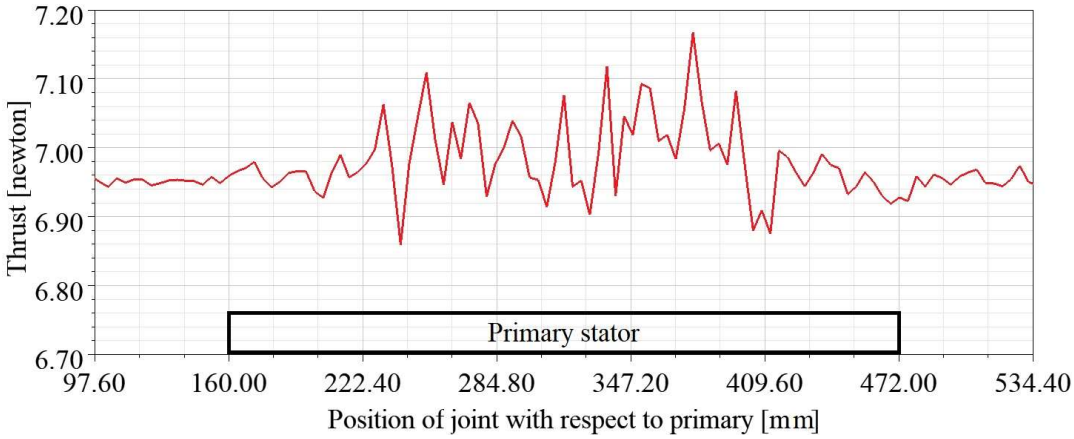

Fig. 5.21 Thrust on the composite secondary vs position of a single joint in the back-iron with respect to LIM Primary

of x-component (and consequent increase of z component) of eddy current. The ripples are due to the combination of slot-tooth effect and the small dimension of the joint. Under dynamic condition the ripple effect gets smoothen out when the joints come appear.

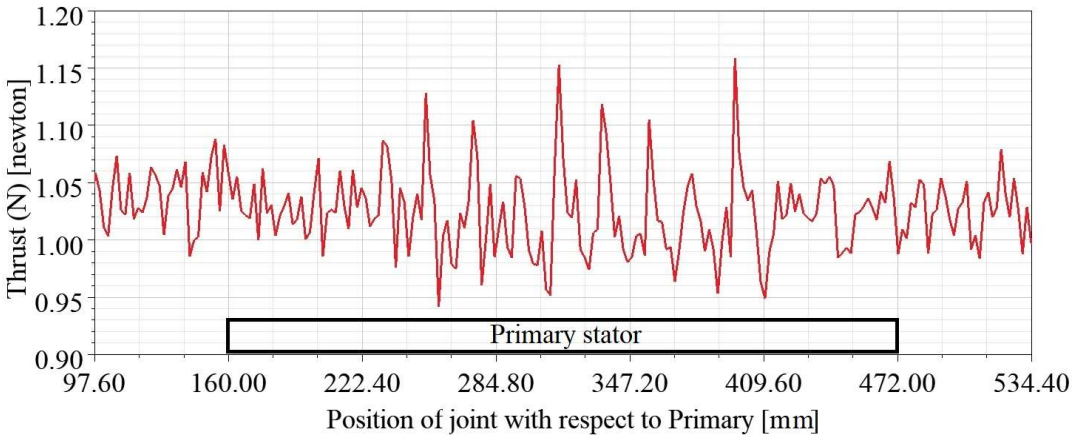

Fig. 5.22 Thrust on the plain secondary vs position of a single joint in the sheet with respect to LIM Primary

Though ripples get pronounced in the case of plain secondary (no back-iron) like in the previous cases when a joint appear, the average thrust gets derated in the absence of back-iron as seen in Fig. 5.22. The average standstill thrust here is comparable to that of Fig. 5.2 at 60 Hz.

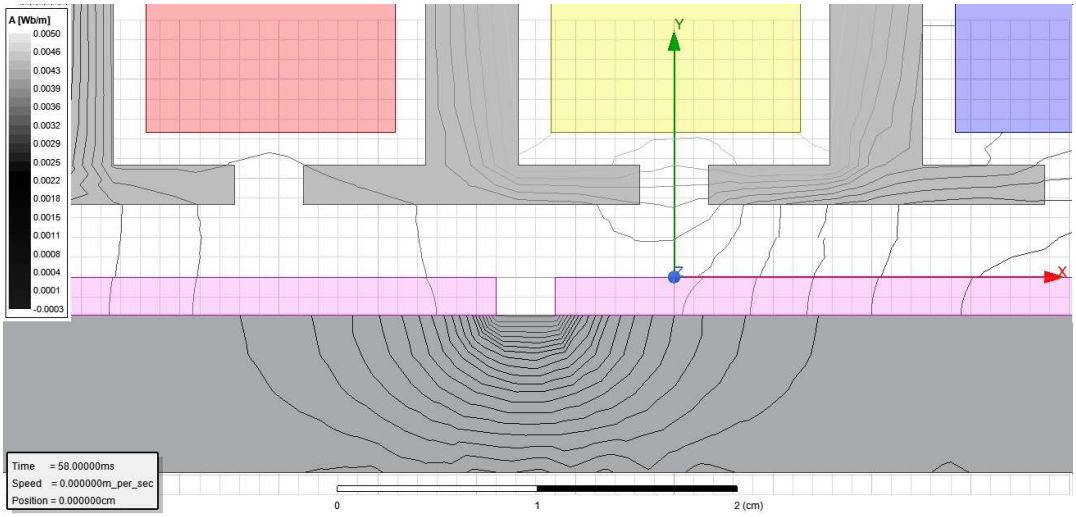

Fig. 5.23 Flux distribution in the back-iron with a joint in the secondary sheet under standstill condition

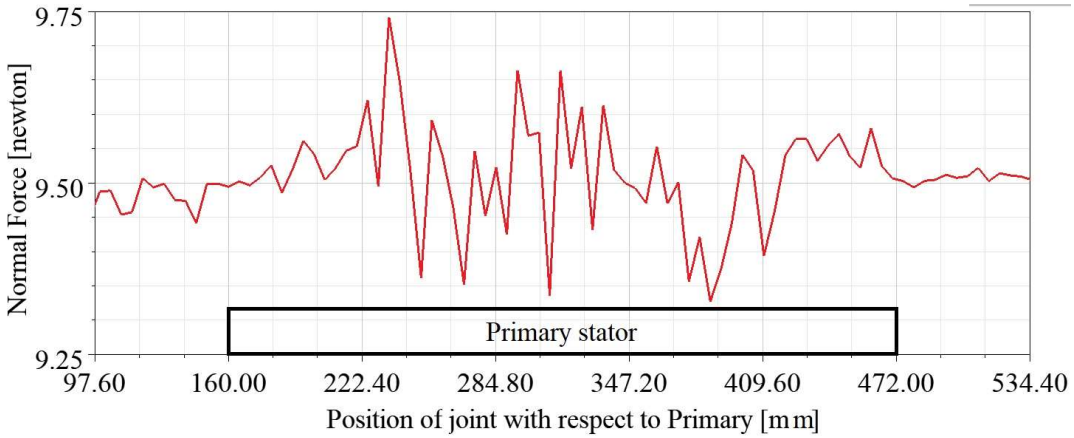

Fig. 5.24 Normal force on the composite secondary vs position of a single joint in the sheet with respect to LIM Primary

A typical crowding of flux in the back-iron under a joint in the secondary sheet in the active zone of the primary is shown in Fig. 5.23.

Normal force behaves differently from thrust under standstill condition when joints are present in the reaction rail. Fig. 5.24 depicts the normal force when a joint is present in the conducting sheet of a composite secondary, while Fig.5.25 pertains to composite

secondary with a joint in the back-iron. Normal force gets swelled when joint is under the first half of the active zone of primary and gets sagged in the latter half.

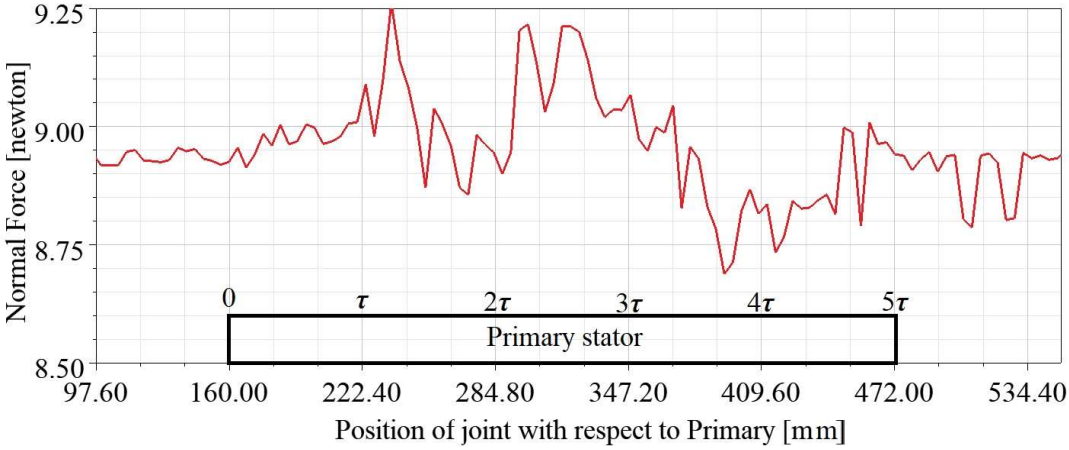

Fig. 5.25 Normal force on the composite secondary vs position of a single joint in the back-iron with respect to LIM Primary

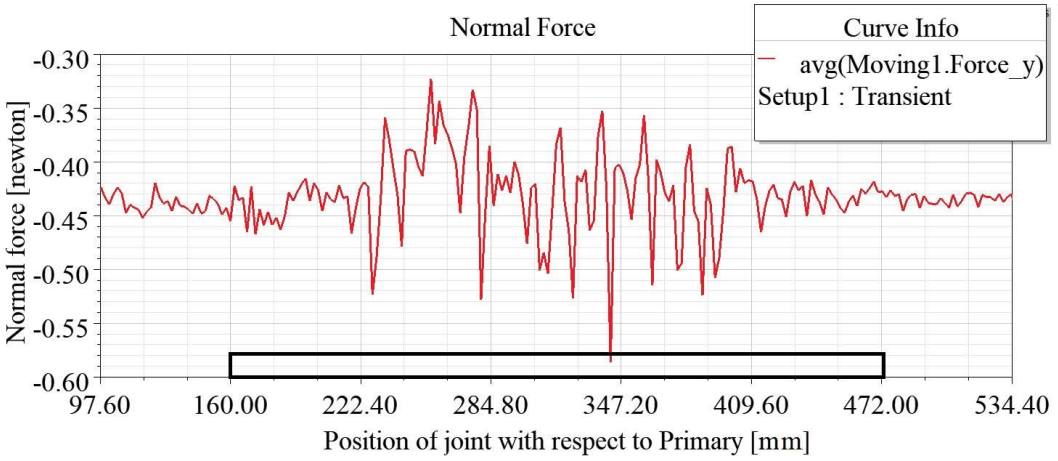

Fig. 5.26 Normal force on the plain secondary vs position of a single joint in the sheet with respect to LIM Primary

Fig. 5.26 depicts normal force on the plain secondary when there is a joint. As expected, normal force is in negative y - direction which is repulsive in nature. Here also the average force gets derated (diminished magnitudes) in the absence of back-iron.

5.4 Effect of presence of ferromagnetic strip jutted out in the air-gap

In this section, the effect of presence of a thin ferromagnetic strip in the clearance has been investigated. The dynamic thrust has been computed for the LIM having ferromagnetic strip in the air clearance. A 2D FEM model of LIM taking slots into account and also having a thin ferromagnetic strip present in the clearance has been developed. The LIM is assumed to have a thin ferromagnetic strip of dimension 3 mm $\times$ 2 mm$\times$ width of SLIM (depth of the 2D model in z-direction) in the transverse direction. It is assumed that the size of strip is not affecting the free movement of SLIM. The schematic 2D model has been shown in Fig. 5.27. The other details of the analyzed LIM are again the same as given in Table 5.1.

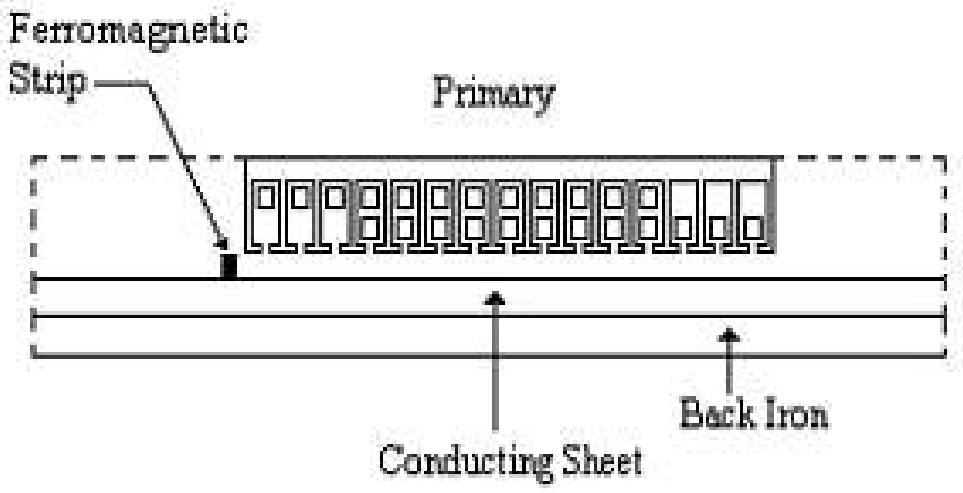

Fig. 5.27 Schematic 2D model of Composite secondary SLIM with a Ferromagnetic Strip in Clearance

The dynamic response of the SLIM in the presence of iron jutted out of a cage type secondary in the air-gap is being obtained in 2D simulation by having a ferromagnetic

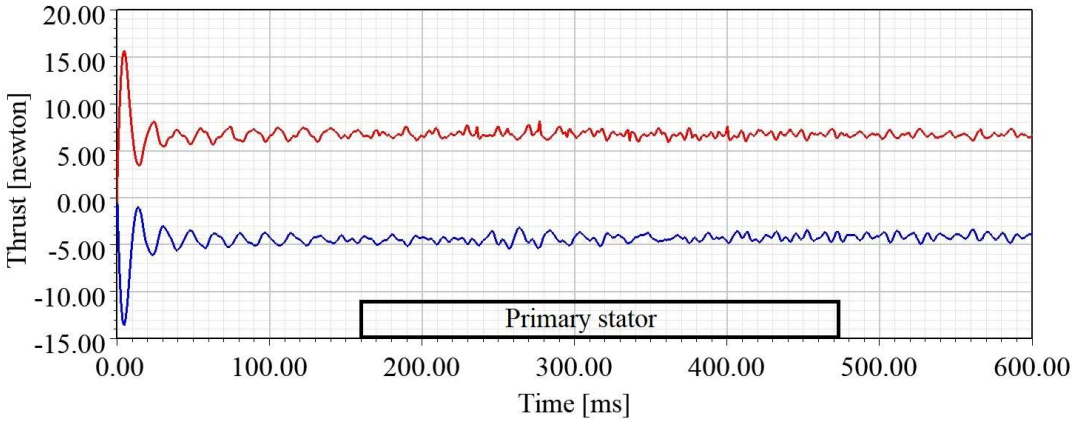

Fig. 5.28 Dynamic thrust for the LIM having ferromagnetic strip in the air clearance

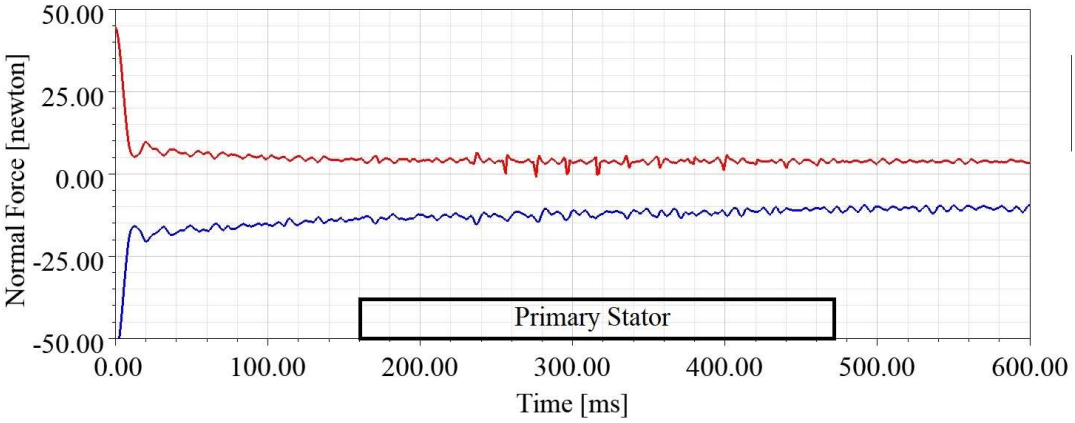

Fig. 5.29 Dynamic Normal force for the LIM having ferromagnetic strip in the air clearance

strip attached to the sheet secondary with back-iron as shown in Fig. 5.27. The thrust (Fig. 5.28) and normal force (Fig. 5.29) response does contain magnified force ripples but there is no change in the average force values when the ferromagnetic strip comes in the air-gap i.e., between the stator and the rotor. The red curves represent forces experienced by the moving secondary, while the blue curves belong to those for the primary stator.

The standstill response of the SLIM also has similar behavior like under dynamic condition.

5.5 Conclusions

The 2-D FEM analysis gives a fairly good picture of the effects of joints in the reaction rail of SLIM. The eddy current patterns in the secondary sheet and back-iron along with flux distribution help in understanding these effects. It can be inferred that the presence of back-iron makes the forces swell when a joint in the secondary comes under the primary. These joints in reaction rail are having comparatively greater significance under dynamic condition as compared to standstill condition. 2Dimensional FEM simulation gives fairly approximate results as far as thrust is concerned, but the results for normal force aren't even close to approximation. A comprehensive 3-D simulation and analytical solution is being envisioned and undertaken to get the accurate picture of the effect of joints. Also, a 3-D simulation of LIM with cage secondary with jutted out iron from the secondary in the air-gap will reveal clearer scenario of the effects than that obtained in this chapter. When machine is being used as a short distance thruster or is at the terminus of transport utility, care must be taken to completely avoid any such joints in the reaction rail. It is suggested that periodic monitoring of the reaction rail should be carried out for the presence of jutted iron in the case of cage type secondary and for the electrical continuity between the jointed sheets in the case of composite or plain secondary.

****